Acta Biochim Biophys Sin 2023, 55(3): 460–471
https://doi.org/10.3724/abbs.2023039
Advance Access Publication Date: 27 March 2023
Original Article

Original Article

AMPK activation attenuates cancer-induced bone pain by reducing mitochondrial dysfunction-mediated neuroinflammation

Heyu Yang[1,†], Yujia Wang[2,†], Shuqing Zhen[3,†], Banghua Wang[1], Ming Jiao[1], Ling Liu[1], Dai Li[1], Haili Zhu[1], and Min Xie[1,*]

[1]Xianning Medical College, Hubei University of Science and Technology, Xianning 437100, China, [2]Xianning Central Hospital, The First Affiliated Hospital of Hubei University of Science and Technology, Xianning 437100, China, and [3]Department of Rheumatism, Matang Hospital of Traditional Chinese Medicine, Xianning 437100, China

[†]These authors contributed equally to this work.

*Correspondence address. Tel: +86-715-8231136; E-mail: xiemin2018@hbust.edu.cn

Received 1 July 2022 Accepted 13 September 2022

Abstract

Bone metastasis of cancer cells leads to severe pain by disrupting bone structure and inducing central sensitization. Neuroinflammation in the spinal cord plays a decisive role in the maintenance and development of pain. In the current study, male Sprague-Dawley (SD) rats are used to establish a cancer-induced bone pain (CIBP) model by intratibial injection of MRMT-1 rat breast carcinoma cells. Morphological and behavioral analyses verify the establishment of the CIBP model, which represents bone destruction, spontaneous pain and mechanical hyperalgesia in CIBP rats. Activation of astrocytes marked by upregulated glial fibrillary acidic protein (GFAP) and enhanced production of the proinflammatory cytokine interleukin-1β (IL-1β) are accompanied by increased inflammatory infiltration in the spinal cord of CIBP rats. Furthermore, activation of the NOD-like receptor pyrin domain-containing protein 3 (NLRP3) inflammasome is consistent with increased neuroinflammation. Adenosine monophosphate-activated protein kinase (AMPK) activation is involved in attenuating inflammatory pain and neuropathic pain. Intrathecal injection of the AMPK activator AICAR in the lumbar spinal cord reduces dynamin-related protein 1 (Drp1) GTPase activity and suppresses NLRP3 inflammasome activation. This effect consequently alleviates pain behaviors in CIBP rats. Cell research on C6 rat glioma cells indicates that AICAR treatment restores IL-1β-induced impairment of mitochondrial membrane potential and elevation of mitochondrial reactive oxygen species (ROS). In summary, our findings indicate that AMPK activation attenuates cancer-induced bone pain by reducing mitochondrial dysfunction-mediated neuroinflammation in the spinal cord.

Key words cancer-induced bone pain, AMPK, AICAR, spinal inflammation, NLRP3-mediated inflammatory signal, mitochondrial dysfunction

Introduction

Global cancer statistics from the International Agency for Research on Cancer (IARC) estimate that in 2020, there were 19.3 million new cancer cases and almost 10 million cancer deaths. It is worth noting that breast cancer is the most commonly diagnosed cancer, with an estimated 2.3 million new cases [1]. In 2022, there will be approximately 4.8 million new cancer cases and 3.2 million cancer deaths in China [2]. With improvements in targeted therapy and immunotherapy, the life expectancy of advanced-stage cancer patients has increased. There is an increased number of cancer patients with bone metastasis; 70% of breast and prostate cancer patients and 20% to 30% of lung or gastrointestinal cancer patients develop bone metastases [3]. Primary bone tumors and bone metastasis disrupt bone structure and stability, which consequently elicits a series of nociceptive stimuli to activate primary afferent fibres. Nociceptive signals are transmitted to the spinal cord and conduct to the supraspinal center, eventually inducing pain perception [4]. Cancer-induced bone pain (CIBP) is a chronic and

unpredictable pathological state that seriously affects patients' physical function and quality of life. The main clinical manifestations of CIBP are background pain, burst pain, and hyperalgesia [5]. Research on the pathological mechanism of CIBP and the development of analgesic drugs are urgently needed.

Neuroinflammation is a cardinal feature of pain and is obviously associated with inflammatory pain, neuropathic pain, cancer pain, and drug treatment-induced pain. Tissue injury and spinal damage cause the release of inflammatory mediators, including proinflammatory cytokines and chemokines. These inflammatory mediators directly stimulate hyperactivity of nociceptive neurons and induce central sensitization, which finally leads to chronic pain [6]. Neuroinflammation is characterized by activated glial cells and increased production of inflammatory mediators. Tumor necrosis factor-α (TNF-α) and interleukin-1β (IL-1β) are the most studied and potent inflammatory cytokines and are mainly produced by microglia and astrocytes in the spinal cord [7]. In arthritis inflammatory pain patients, functional MRI analysis demonstrated that neutralization of TNF-α blocked nociceptive signals of the central nervous system elicited by arthritis [8]. Postmortem examination of pain-positive HIV patients showed increased TNF-α and IL-1β, especially in the spinal dorsal horn. Meanwhile, the expression of the astrocytic markers glial fibrillary acidic protein (GFAP) and S100β was also upregulated [9]. In our previous research, we found that spinal neuroinflammation was enhanced both in rat models of complete Freund's adjuvant (CFA)-induced inflammatory pain and in cancer-induced bone pain [10,11]. It is important to note that inhibition of neuroinflammation could be a potential therapeutic strategy for pathological pain.

Mitochondrial dysfunction and production of reactive oxygen species (ROS) are critically involved in the pain process. During the resolution of inflammatory pain, sensory neurons are sensitized to stress, and the macrophages that infiltrate the dorsal root ganglia (DRG) transfer mitochondria to the somata of sensory neurons, which recover oxidative phosphorylation [12]. In animals with chemotherapy-induced neuropathic pain, abnormal swollen and vacuolated mitochondria, increased cellular ROS, and mitochondrial superoxide production were observed [13]. In mice of the HIV-infected pain model, systemic application of the ROS scavenger blocked astrocytic activation and relieved pain behavior induced by morphine treatment [14]. For neuropathic pain, the number of damaged mitochondria was increased, and the mean planar mitochondrial area was decreased in a chronic contractile injury rat model. Accordingly, targeting the regulation of mitochondrial function is favorable for chronic pain treatment.

Adenosine monophosphate-activated protein kinase (AMPK) is a cellular energy sensor that governs mitochondrial morphology and localization [15]. It was reported that activation of AMPK phosphorylated dynamin-related protein 1 (Drp1) at Ser637, which prevented mitochondrial fission and attenuated mitochondrial fragmentation [16,17].

In the current study, to investigate the effect of AMPK on cancer pain, the AMPK activator AICAR was injected into the spinal cord of CIBP rats, and spinal inflammation and pain behaviors were subsequently detected. This study aimed to clarify the mechanism of AMPK activation in the alleviation of cancer pain and provide a potential analgesic target for cancer-induced bone pain management.

Materials and Methods

Antibodies and reagents

The AMPK activator AICAR (S1802), NLRP3 inhibitor MCC950 (S8930), and Drp1 inhibitor Mdivi-1 (S7162) were purchased from Selleck Chemicals (Houston, USA). Anti-GFAP antibody (ab4648) was purchased from Abcam (Cambridge, UK); NLRP3 rabbit pAb (A12694), Caspase-1 rabbit pAb (A0964), IL-1β rabbit pAb (A1112), NLRP1 rabbit pAb (A16212) and NLRC4 rabbit pAb (A7382) were purchased from ABclonal Technology (Wuhan, China); AMPK alpha antibody (AF6423), phospho-AMPK alpha (Thr172) antibody (AF3423), Drp1 antibody (DF7073), phospho-Drp1 (Ser637) antibody (DF2980), phospho-Drp1 (Ser616) antibody (AF8470), AIM2 antibody (DF3514) and β-actin antibody (AF7018) were purchased from Affinity Biosciences (Changzhou, China). A mitochondrial membrane potential assay kit with JC-1 (C2006) was purchased from Beyotime (Shanghai, China). MitoSOX™ Red mitochondrial superoxide indicator was purchased from Thermo Fisher Scientific (Waltham, USA). RPMI 1640 medium, Dulbecco's modified Eagle's medium (DMEM), fetal bovine serum (FBS), Pen Strep (penicillin-streptomycin), and trypsin were obtained from Gibco (Carlsbad, USA).

Cell culture and treatment

MRMT-1 rat mammary gland carcinoma cells (Jennio Biotech, Guangzhou, China) were cultured in RPMI 1640 medium supplemented with 10% FBS, 50 U/mL penicillin, and 50 μg/mL streptomycin. On the day of surgery, MRMT-1 cells were collected by centrifugation, and the pellet was resuspended in Hank's balanced salt solution (HBSS) and kept on ice until use. C6 rat glioma cells (Jennio Biotech) were seeded in DMEM with 10% FBS, 50 U/mL penicillin, and 50 μg/mL streptomycin. For mitochondrial membrane potential and mitochondrial ROS analysis, C6 cells were treated with 0 and 1 μM AICAR for 24 h, digested with trypsin, and collected for western blot analysis. AICAR was dissolved in dimethyl sulfoxide (DMSO).

Establishment of the CIBP rat model and treatment

Thirty-six male Sprague–Dawley (SD) rats weighing 180 ~ 200 g (6–8 weeks old) were purchased from the Hubei Province Experimental Animal Center (Wuhan, China). Animals were housed in a 12/12 h light-dark cycle regime and temperature-controlled room (22 ± 1°C), with access to water and food ad libitum. All efforts were made to minimize the animals' suffering. The animal experiments in this study were approved by the Experimental Animal Ethics Committee of Hubei University of Science and Technology (2019-03-021). Rats were randomly divided into four groups: sham group, AICAR-treated group, CIBP group and AICAR-treated CIBP group. Each group contained nine rats. The rats were acclimated to the environment for 5 days prior to the experiments. The rats in the CIBP and CIBP + AICAR groups were used to establish the CIBP model. To imitate cancer bone metastasis, MRMT-1 cells were inoculated into the intramedullary space of the rat tibia to establish a model of cancer-induced bone pain. Briefly, animals were anaesthetized with an intraperitoneal injection of pentobarbital sodium (50 mg/kg), and the left hind limb was shaved and disinfected with 70% ethanol. Then, a hole was drilled in the left tibia, and a microsyringe with 3.5×10^5 cells in HBSS was slowly injected into the intramedullary space. The sham and AICAR rats were injected with an equivalent volume of vehicle

(HBSS). After the CIBP animal model was established, rats from the AICAR and CIBP + AICAR groups were intrathecally treated with the AMPK activator AICAR. Briefly, a microsyringe with 10 μL AICAR (1 mg/kg) was inserted between the L5 and L6 vertebrae and injected slowly. AICAR was dissolved in DMSO and diluted with 0.9% NaCl (v/v = 1:1) before use. The sham and CIBP rats were injected with the same volume (10 μL) of vehicle (DMSO and 0.9% NaCl).

Bone X-ray and histological analysis

Roentgenography of the ipsilateral tibia was performed on the 14th day after inoculation of MRMT-1 cells. Legs were placed on X-ray film and exposed to an X-ray source. Tumor cell infiltration and bone destruction were detected by hematoxylin and eosin (H&E) staining. Briefly, on day 14 after surgery, rats were euthanized with an overdose of pentobarbital sodium (100 mg/kg, i.p.), and then the left tibia were collected, fixed in 4% paraformaldehyde for 24 h and decalcified using 10% EDTA solution. Finally, the bone tissue was dehydrated and embedded in paraffin and cut into 4-μm sections using a Shandon Finesse E+ rotary microtome (Thermo Fisher Scientific). The sections were stained with H&E. Images were acquired with an IX73 fluorescence microscope (Olympus, Tokyo, Japan).

Pain behavioral assay

The rats in the sham, AICAR, CIBP, and CIBP + AICAR groups (nine for each group) were subjected to behavioral testing after drug treatment. Cancer-induced spontaneous pain was observed as flinching or licking of the left hind paw of rats. Rats were placed in individual polyvinyl boxes, and spontaneous pain was measured in 5-min intervals. For measurement of mechanical allodynia, rats were habituated to testing equipment, a polyvinyl box on a wire mesh platform, and allowed to adapt for 30 min. The paw withdrawal threshold (PWT) was measured using von Frey filaments (ranging from 0.4 g to 26 g) to stimulate the left hind paw. Briefly, the filaments were pressed vertically against the plantar surfaces until the filaments were bent and held for 6-8 s. Brisk withdrawal and paw flinching were considered positive responses. Whenever a positive response occurred, the von Frey filament with the next lower force was applied, and whenever a negative response occurred, the filament with the next higher force was applied. Then, the pattern of positive and negative withdrawal responses was converted to a 50% PWT.

Western blot analysis

After 6 h of AICAR and vehicle administration, the rats in the sham, CIBP and CIBP + AICAR groups (three rats for each group) were sacrificed. The spinal cord was removed and collected into ice-cold RIPA lysis buffer containing a cocktail of protease inhibitors and homogenized on ice. The homogenate was centrifuged at 12,000 *g* for 15 min, and the supernatant was collected for western blot analysis. The protein concentration was determined using a BCA kit (Beyotime, Shanghai, China). Equal amounts of protein samples were separated by 10% SDS-PAGE and electrically transferred onto PVDF membranes (Millipore, Billerica, USA). Then, the membranes were blocked with QuickBlock™ Blocking Buffer for Western Blot (Beyotime) and incubated with the appropriate primary antibodies overnight at 4°C. The following primary antibodies were used: GFAP (1:1000), NLRP3 (1:1000), caspase-1 (1:1000), IL-1β (1:1000), NLRP1 (1:1000), NLRC4 (1:1000), TNF-α (1:1000), AMPK alpha (1:1000), phospho-AMPK alpha (Thr172) (1:1000), Drp1 (1:1000), phospho-Drp1 (Ser637) (1:1000), phospho-Drp1 (Ser616) (1:1000), AIM2 (1:1000), and β-actin (1:50,000). After incubation with goat anti-rabbit IgG (H + L)-HRP or goat anti-mouse IgG (H + L)-HRP, the membranes were visualized with iBright 1500 (Invitrogen, Carlsbad, USA). The bands were analysed using ImageJ software (NIH, Bethesda, USA).

Histology and immunofluorescence analysis of the spinal cord

After drug administration, rats (three for each group) were deeply anaesthetized and perfused with 4% paraformaldehyde. Spinal cords from treated rats were removed and postfixed for 12 h. After embedment in paraffin, the tissues were cut into 4-μm sections using a microtome. The tissue sections were then stained with H&E and imaged with a microscope. For the immunofluorescence assay, spinal cord sections were dewaxed, boiled at 95°C in antigen repair solution for 15 min and left to cool naturally to an appropriate temperature. Then, the sections were incubated with 3% H_2O_2 solution and blocked with immunofluorescence blocking solution. Subsequently, the sections were incubated with primary antibodies against IL-1β (1:100), GFAP (1:100), AMPK alpha (1:100), Drp1 (1:100), NLRP3 (1:100), and Caspase-1 (1:100). After three washes, the sections were incubated with goat-rabbit IgG H&L (FITC) and goat-mouse IgG H&L (TRITC). Then, the sections were mounted with antifade mounting medium. Images were acquired with the IX73 fluorescence microscope (Olympus). The fluorescence intensity was analysed using ImageJ software (NIH).

Transmission electron microscopy (TEM)

After administration, spinal cord tissues were collected (three rats for each group), and mitochondria in the spinal cord were confirmed by electron microscopy of negatively stained samples. Briefly, the spinal cord was isolated, cut into ~1 mm^3 cubes, fixed in 2.5% glutaraldehyde, and postfixed with 1% osmium tetroxide. Ultrathin sections were poststained with uranyl acetate and lead citrate and then examined with an HC-1 transmission electron microscope (Hitachi, Tokyo, Japan) operating at 120 kV.

Mitochondrial membrane potential (MMP) measurement

For the cell experiment, C6 cells were seeded onto sterilized coverslips placed in 24-well plates. After IL-1β induction for 2 h, AICAR (1 μM), Mdivi-1 (1 μM) and MCC950 (1 μM) were added to the medium and incubated for 24 h. After treatment, a JC-1 assay was performed to evaluate MMP. Briefly, cells were washed with ice-cold PBS and incubated with JC-1 solution for 20 min at 37°C in the dark. Then, the cells were washed with JC-1 staining buffer, and culture medium was added. The fluorescence of monomers (green) and aggregates (red) was observed with the IX73 fluorescence microscope (Olympus). CCCP (carbonyl cyanide 3-chlorophenylhydrazone) was used as a positive control for inducing a reduction in mitochondrial membrane potential. The fluorescence intensity was analysed using ImageJ software (NIH).

Mitochondrial reactive oxygen species assessment

MitoSOX-based assays were used to detect mitochondrial ROS. MitoSOX red mitochondrial superoxide indicator is a novel fluorogenic dye for highly selective detection of superoxide in the

mitochondria of live cells. The detection followed the manufacturer's protocols. Briefly, cells were inoculated in a 24-well plate, IL-1β induction (2 h) was performed prior to AICAR (1 μM, 24 h), Mdivi-1 (1 μM, 24 h) and MCC950 (1 μM, 24 h) treatment. Subsequently, the cells were incubated with 5 μm MitoSOX in the dark at 37°C for 10 min and imaged with the IX73 fluorescence microscope (Olympus). The fluorescence intensity was analysed using ImageJ software (NIH).

Statistical analysis

All statistical analyses were conducted with the SPSS 21.0 software package. The analysis of PWT, flinches, spinal H&E staining, immunofluorescence, and TEM observation between two experimental groups was performed using unpaired Student's *t* test. The PWT, flinches, and western blot analysis of the sham, CIBP and CIBP + AICAR groups were analysed by one-way analysis of variance (one-way ANOVA) followed by Tukey's test. The JC-1 mitochondrial membrane potential and mitochondrial ROS among the five groups were analysed by one-way ANOVA followed by Tukey's test. Data are presented as the mean ± SD. $P < 0.05$ was considered statistically significant.

Results

AICAR treatment relieves cancer-induced pain behaviors

The establishment and behavior tests were conducted according to the processes shown in Figure 1A. To investigate the effect of AICAR on cancer-induced bone pain, a CIBP rat model was established by tibial inoculation of MRMT-1 cells. The model was validated by pain behavior tests and radiological and histological analyses. X-ray radiographs exhibited tibial destruction of CIBP rats on postsurgery day 14, while there was no obvious structural destruction in the sham group (Figure 1B). Histological analysis of the tibia showed increased cell infiltration in bone marrow spaces and loss of normal bone structure, which was characterized by a deficiency of trabecular bone in the CIBP group. Nevertheless, well-organized trabecular bone was observed in the sham group (Figure 1C).

To evaluate the pain behavior induced by cancer inoculation, spontaneous flinches and mechanical pain thresholds were detected. Compared with the sham group, mechanical pain sensitivity, presented as the PWT value, was significantly decreased in the CIBP rats. The ipsilateral hind paw PWT value decreased from 15.14 ± 3.07 g on day 0 (before cell inoculation) to 6.85 ± 1.58 g on day 7 (after inoculation, $P < 0.05$ vs sham group) and 5.8 ± 1.44 g on day 14 (after inoculation, $P < 0.05$ vs sham, Figure 1D). Consistent with the increased mechanical pain behavior, spontaneous pain behavior also increased in CIBP rats. Spontaneous pain was measured by spontaneous flinches, and the results showed that the number of spontaneous flinches per 5 min in CIBP rats increased from 6.77 ± 2.17 on day 0 to 21.3 ± 2.78 on day 7 ($P < 0.05$ vs sham group) and 27.44 ± 3.97 on day 14 ($P < 0.05$ vs sham, Figure 1E). These data indicated that intratibial inoculation of MRMT-1 cells induced bone damage and pain hyperalgesia.

To explore the effect of AMPK activation on the pain behavior of CIBP rats, the AMPK activator AICAR was intrathecally injected into the lumbar spinal cord of CIBP rats. In contrast to the CIBP group, 3 h (CIBP vs CIBP + AICAR: 6.82 ± 1.89 vs 12.28 ± 1.99) and 6 h (CIBP vs CIBP + AICAR: 5.29 ± 2.23 vs 13.18 ± 1.75) of AICAR treatment significantly increased PWT values ($P < 0.05$ vs CIBP group, Figure 1F). In addition, AICAR treatment significantly decreased the number of spontaneous flinches ($P < 0.05$ vs CIBP group). The numbers of spontaneous flinches in the CIBP group and CIBP + AICAR group at 3 h after AICAR treatment were 29.89 ± 2.85 and 15.42 ± 2.47, respectively, and at 6 h were 15.44 ± 2.46 and 16.44 ± 3.2, respectively (Figure 1G). AICAR treatment had no obvious effect on the pain behaviors of normal rats ($P > 0.05$ vs control group, Figure 1F,G). These data suggested that AICAR treatment alleviated cancer-induced mechanical allodynia and spontaneous pain.

AICAR reduces spinal inflammation

Neuroinflammation in the spinal cord plays a decisive role in pain development and persistence [18]. Inflammatory infiltration detected by H&E staining in spinal cord sections showed that cell infiltration in CIBP rats was higher than that in sham rats, especially in the spinal dorsal horn, and the relative inflammation score of the CIBP group was 2.83 ± 0.31 ($P < 0.05$ vs sham group, Figure 2A,B). The proinflammatory cytokine IL-1β is a key mediator of the inflammatory response and is implicated in pain [7]. Herein, the expression of IL-1β in the spinal dorsal horn represented neuroinflammation in CIBP rats. The fluorescence intensity of IL-1β was enhanced in the spinal dorsal horn of CIBP rats, with a relative intensity of 2.23 ± 0.06 ($P < 0.05$ vs sham group, Figure 2C,D). Activation of astrocytes leads to an inflammatory response, and GFAP is one of the best markers for activated astrocytes [9]. Immunofluorescence analysis showed that the fluorescence intensity of GFAP in the spinal dorsal horn was obviously increased in the CIBP group, with a relative intensity of 1.83 ± 0.07 ($P < 0.05$ vs sham group, Figure 2E,F).

To investigate the anti-inflammatory effect of AICAR, the protein expression levels of IL-1β and GFAP were measured by western blot analysis. The upregulated levels of IL-1β and GFAP in the spinal cord of CIBP rats were reduced by AICAR treatment ($P < 0.05$ vs CIBP group, Figure 2G,H). The relative levels of IL-1β in the CIBP group and CIBP + AICAR group were 2.37 ± 0.14 and 1.76 ± 0.1, respectively; the relative levels of GFAP in the CIBP group and CIBP + AICAR group were 2.58 ± 0.12 and 1.34 ± 0.15, respectively. These data illustrated that AICAR treatment suppressed astrocyte-mediated neuroinflammation in the spinal cord of CIBP rats.

AMPK activation decreases Drp1 activity

It was reported that activation of AMPK increased Drp1 localization at the mitochondrial outer membrane and prevented mitochondrial fission by enhancing Drp1 phosphorylation at Ser637. Ser637 is an inhibitory site of Drp1 GTPase activity that reduces its translocation to mitochondria [19]. In addition, phosphorylation of Drp1 at Ser616 promotes Drp1-mediated mitochondrial fission [20]. In the present study, we detected the effect of AMPK activation on spinal Drp1 activity. Immunofluorescence analysis showed that the fluorescence intensity of AMPK in the spinal dorsal horn was significantly lower in the CIBP group than in the sham group. The relative fluorescence intensity of AMPK in the CIBP group was 0.7 ± 0.09 ($P < 0.05$ vs sham group, Figure 3A,C). Additionally, the fluorescence intensity of Drp1 in the spinal dorsal horn of the CIBP group was increased (1.81 ± 0.15) compared with that in the sham group ($P < 0.05$ vs sham group, Figure 3B,C). Furthermore, mitochondrial morphology in the spinal cord of sham and CIBP rats was detected by TEM. For the sham group, the mitochondrial structure exhibited a whole compact outer membrane and normal

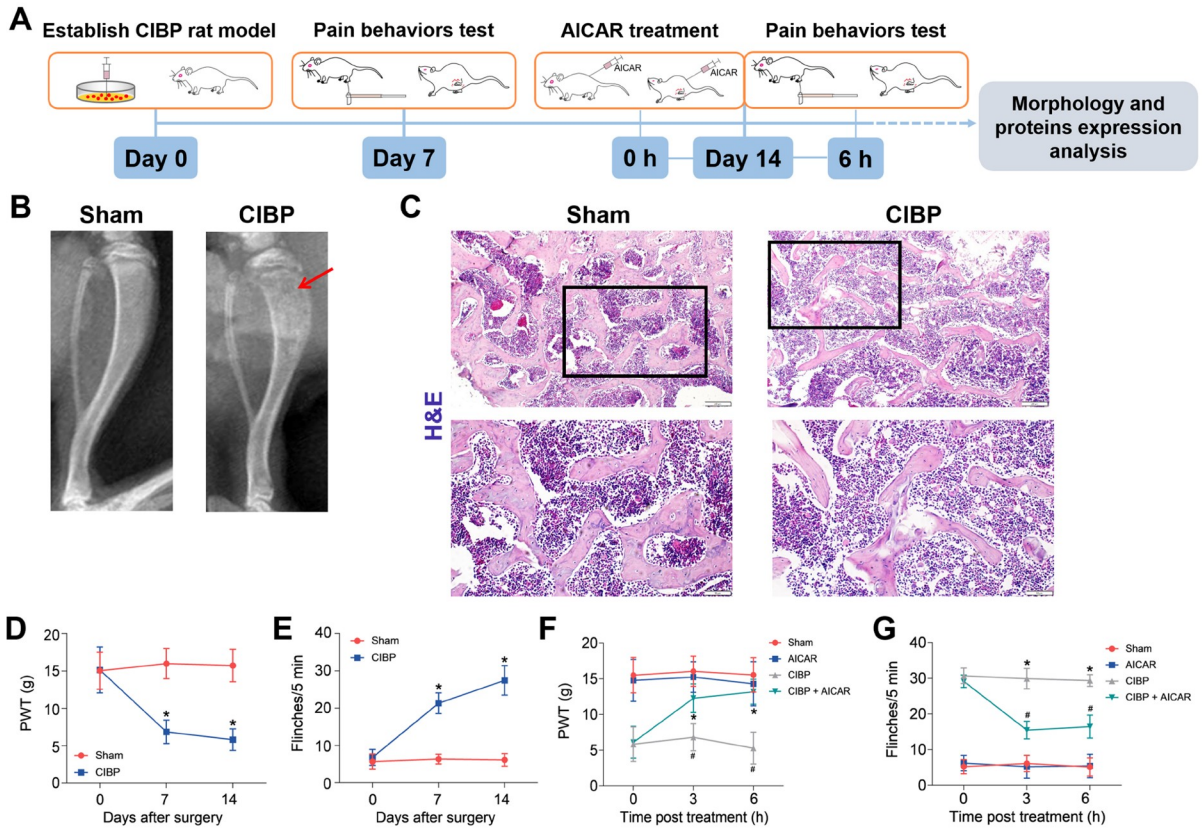

Figure 1. Effect of AICAR treatment on bone morphology and pain behaviors (A) Schematic diagram of the experimental procedures. Before the surgery, the rats were allowed to acclimatize for at least 7 days. The detection of pain behavior was performed at 0, 7, and 14 days after the inoculation of cancer cells. On day 14 after the surgery, AICAR was injected into the lumbar spinal cord, and subsequently, the rats were sacrificed, and the tissues were collected for further analysis. (B) Representative radiographs of the ipsilateral tibia from sham and CIBP rats on day 14 after inoculation of Hank's solution or cancer cells. The red arrows indicate areas of bone destruction in CIBP rats. (C) Representative images of H&E staining of tibial sections from sham and CIBP rats. The below panel shows zoomed images of the above panel marked with black rectangles. Scale bars: first panel, 100 μm; second panel, 50 μm. (D,E) Evaluation of pain behaviors in sham and CIBP rats with PWT values and spontaneous flinches. Data are expressed as the mean ± SEM ($n = 9$). *$P < 0.05$ vs sham group. (F,G) Changes in PWT values and spontaneous flinches after vehicle and AICAR treatment in control and CIBP rats. Data are expressed as the mean ± SEM ($n = 9$). *$P < 0.05$ vs sham group, #$P < 0.05$ vs CIBP group.

cristae. In contrast, mitochondria in the CIBP group were disrupted, and discontinuous outer membranes and deficient cristae were observed (Figure 3D). The number of damaged mitochondria in the CIBP group was higher than that in the sham group, and the relative ratios of damaged mitochondria in the sham and CIBP groups were 1.0% ± 0.14% and 2.4% ± 0.23%, respectively ($P < 0.05$ vs sham group, Figure 3E).

AMPK phosphorylation at Thr172 positively regulates AMPK activity. Herein, the level of phosphorylated AMPK in the spinal cord was detected by western blot analysis. The data showed a decrease in spinal phosphorylation of AMPK at Thr172 in the CIBP group, while AICAR treatment upregulated phosphorylated AMPK. The relative activity of AMPK was represented by the phosphorylated AMPK (Thr172)/AMPK ratio, and the values of the CIBP group and CIBP + AICAR group were 0.53 ± 0.1 and 0.95 ± 0.18, respectively ($P < 0.05$ vs CIBP group, Figure 3F,G). Moreover, AICAR treatment increased the phosphorylation of Drp1 at Ser637 (decreased in CIBP) but reduced the phosphorylation of Drp1 at Ser616 (upregulated in CIBP). The relative activity of Drp1 was represented by the phosphorylated Drp1 (Ser637)/Drp1 ratio or phosphorylated Drp1 (Ser616)/Drp1 ratio. The Drp1 (Ser637)/Drp1 ratios in the CIBP group and CIBP + AICAR group were 0.42 ± 0.11 and 1.28 ± 0.04, respectively; the Drp1 (Ser616)/Drp1 ratios were 1.82 ± 0.12 and 1.37 ± 0.11, respectively ($P < 0.05$ vs CIBP group, Figure 3F,G). These results suggested that AMPK activation reduced Drp1-mediated mitochondrial fission activity in CIBP rats.

AMPK activation inhibits NLRP3 inflammasome activation

The NOD-like receptor family pyrin domain-containing 3 (NLRP3) inflammasome mediates caspase-1 activation and IL-1β maturation and secretion, and consequently participates in neuroinflammation [21]. Immunofluorescence analysis showed that the relative fluorescence intensities of NLRP3 (1.66 ± 0.16, $P < 0.05$ vs sham group, Figure 4A,B) and caspase-1 (2.18 ± 0.08, $P < 0.05$ vs sham group, Figure 4C,D) in the spinal dorsal horn of the CIBP group were higher than those in the sham group. Consistent with immunofluorescence analysis, western blot analysis also indicated elevated protein levels of NLRP3 and activated caspase-1 in the spinal cord of CIBP rats compared with the sham group. The relative levels of NLRP3 and activated caspase-1/caspase-1 in CIBP rats were 1.46 ± 0.12 and 2.08 ± 0.13, respectively ($P < 0.05$ vs sham group, Figure 4E,F). AICAR treatment reduced the upregulation of NLRP3 and activated caspase-1 levels; the relative level of NLRP3 was

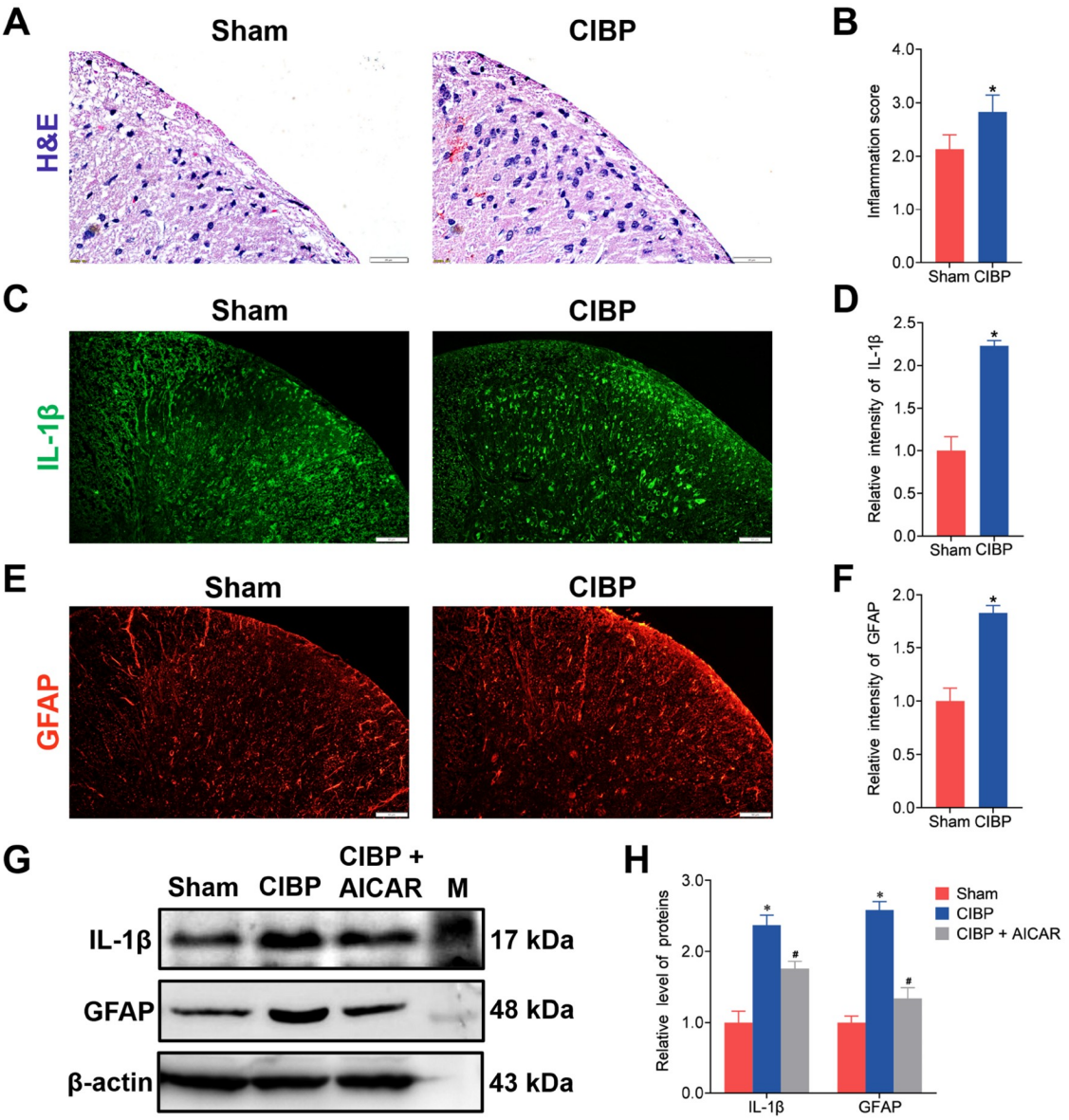

Figure 2. Effect of AICAR treatment on inflammatory infiltration and levels of IL-1β and GFAP in the spinal cord (A) Representative H&E staining images of spinal cord sections from the sham group and CIBP group. Scale bar: 20 μm. (B) Quantitative analysis of H&E staining in each group represented by the inflammation score. Data are expressed as the mean ± SD ($n = 3$). *$P < 0.05$ vs sham rats. (C,E) Representative immunofluorescence staining images show the expression of IL-1β and GFAP in the spinal dorsal horn of sham and CIBP rats. Scale bar: 20 μm. (D,F) Quantitative analysis of fluorescence intensity in (C) and (E). Data are expressed as the mean ± SD ($n = 3$). *$P < 0.05$ vs sham group. (G) Western blot analysis of the levels of IL-1β and GFAP in the spinal cord of the sham, CIBP, and CIBP + AICAR groups. (H) Quantification of the relative protein levels in (G). Data are presented as the mean ± SD ($n = 3$). *$P < 0.05$ vs sham group, #$P < 0.05$ vs CIBP group.

0.76 ± 0.08, and the activated caspase-1/caspase-1 ratio was 1.21 ± 0.1 ($P < 0.05$ vs CIBP group, Figure 4E,F). Since other inflammasomes, including NLRP1, NLR family CARD domain-containing protein 4 (NLRC4) and absent in melanoma 2 (AIM2), can also mediate caspase-1 activation and mature IL-1β production, we detected the expressions of these inflammasomes by western blot analysis. As shown in Figure 4G,H, the level of NLRP1 was increased in CIBP rats, and AICAR treatment had an obvious inhibitory effect on NLRP1 expression. In contrast to NLRP1, the levels of NLRC4 and AIM2 did not show significant differences among the sham, CIBP and CIBP + AICAR groups. Combined with Figure 2, these data indicated that AMPK activation suppressed spinal neuroinflammation by the NLRP3 inflammasome.

AMPK activation restores mitochondrial function in C6 cells

To verify the effect of AMPK activation on inflammation, the AMPK activator AICAR and inhibitor dorsomorphin were used to treat C6 cells. Next, the levels of AMPK, Drp1 and NLRP3 were detected by western blot analysis. As shown in Figure 5A,B, AICAR increased the phosphorylation of AMPK at Thr172 and Drp1 at Ser637 and decreased the phosphorylation of Drp1 at Ser616. Dorsomorphin has the opposite effect on the phosphorylation of AMPK and Drp1. Subsequently, the mitochondrial membrane potential (MMP) and

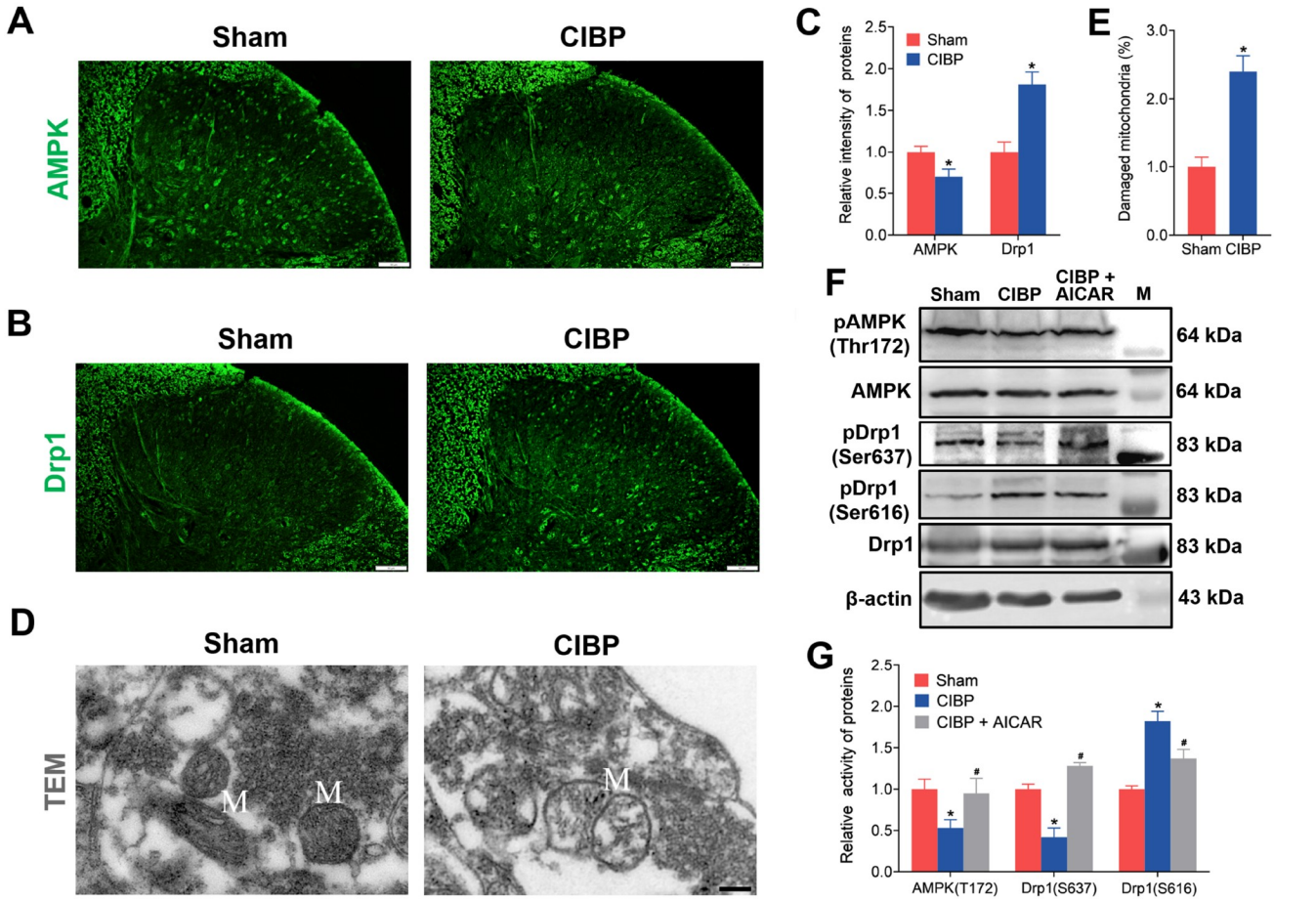

Figure 3. Effect of AICAR treatment on the activities of AMPK and Drp1 (A,B) Representative immunofluorescence staining images of the expression of AMPK and Drp1 in the spinal dorsal horn of sham and CIBP rats. Scale bar: 20 μm. (C) Quantitative analysis of fluorescence intensity in (A) and (B). Data are expressed as the mean ± SD ($n = 3$). *$P < 0.05$ vs sham group. (D) Representative TEM images of spinal mitochondria from sham and CIBP rats. M: mitochondria; Scale bar: 200 nm. (E) Quantitative analysis of the damaged mitochondrial ratio in (D). Data are expressed as the mean ± SD ($n = 3$). *$P < 0.05$ vs sham group. (F) Western blot analysis of the levels of phosphorylated AMPK (Thr172), total AMPK, phosphorylated Drp1 (Ser637 and Ser616), and total Drp1 in the spinal cord of the sham, CIBP, and CIBP + AICAR groups. β-Actin was used as a loading control. (G) Quantification of the relative protein levels in (F). The relative level of phosphorylated AMPK was normalized to total AMPK; phosphorylated Drp1 was normalized to total Drp1. Data are presented as the mean ± SD ($n = 3$). *$P < 0.05$ vs sham group, #$P < 0.05$ vs CIBP group.

mitochondrial ROS were detected in inflammation-induced C6 rat glioma cells. C6 cells were treated with IL-1β to induce inflammation before examination. Changes in mitochondrial membrane potential were detected by JC-1 staining. Compared with the control group, IL-1β induction led to significantly lower red fluorescence intensity and higher green fluorescence, which suggested a reduced MMP, while AICAR treatment increased mitochondrial MMP. Moreover, to further confirm the effect of AMPK activation on MMP, the mitochondrial fission inhibitor Mdivi-1 was used to treat IL-1β-induced cells. The increased red fluorescence intensity indicated restored MMP compared with the IL-1β group. The NLRP3 inhibitor MCC950 was also used to detect whether NLRP3 inhibition influenced MMP. The results showed that MCC950 also improved the MMP of IL-1β-induced cells. The relative ratios of red/green fluorescence in the IL-1β, IL-1β + AICAR, IL-1β + Mdivi-1 and IL-1β + MCC950 groups were 0.35 ± 0.03, 0.88 ± 0.06, 0.96 ± 0.06 and 0.64 ± 0.05, respectively ($P < 0.05$ vs control group or IL-1β group, Figure 5C,E). Next, changes in mitochondrial ROS production were detected using MitoSOX. Mitochondrial ROS were dramatically increased by IL-1β induction, and AICAR treatment reduced IL-1β-induced high intensity. The intensity of Mdivi-1-treated IL-1β-induced cells was also decreased, while MCC950 had no effect on mitochondrial ROS. The relative mitochondrial ROS fluorescence intensities were IL-1β, 1.44 ± 0.04; IL-1β + AICAR, 0.99 ± 0.05; IL-1β + Mdivi-1, 1.08 ± 0.06; and IL-1β + MCC950, 1.41 ± 0.04 ($P < 0.05$ vs control group or IL-1β group, Figure 5D,F). These data indicated that AMPK activation significantly reversed inflammation-induced mitochondrial membrane potential deficiency and high mitochondrial ROS contents.

Discussion

Pain is an unpleasant perception that often accompanies tissue injury, infection, cancer, and inflammatory diseases [22]. Cancer-induced bone pain is chronic pain with a complicated pathogenesis. It can be caused by local pressures by increasing tumor sizes and substances produced by tumor cells [4]. This damage to the periphery stimulates noxious signals and sensitizes the spinal cord.

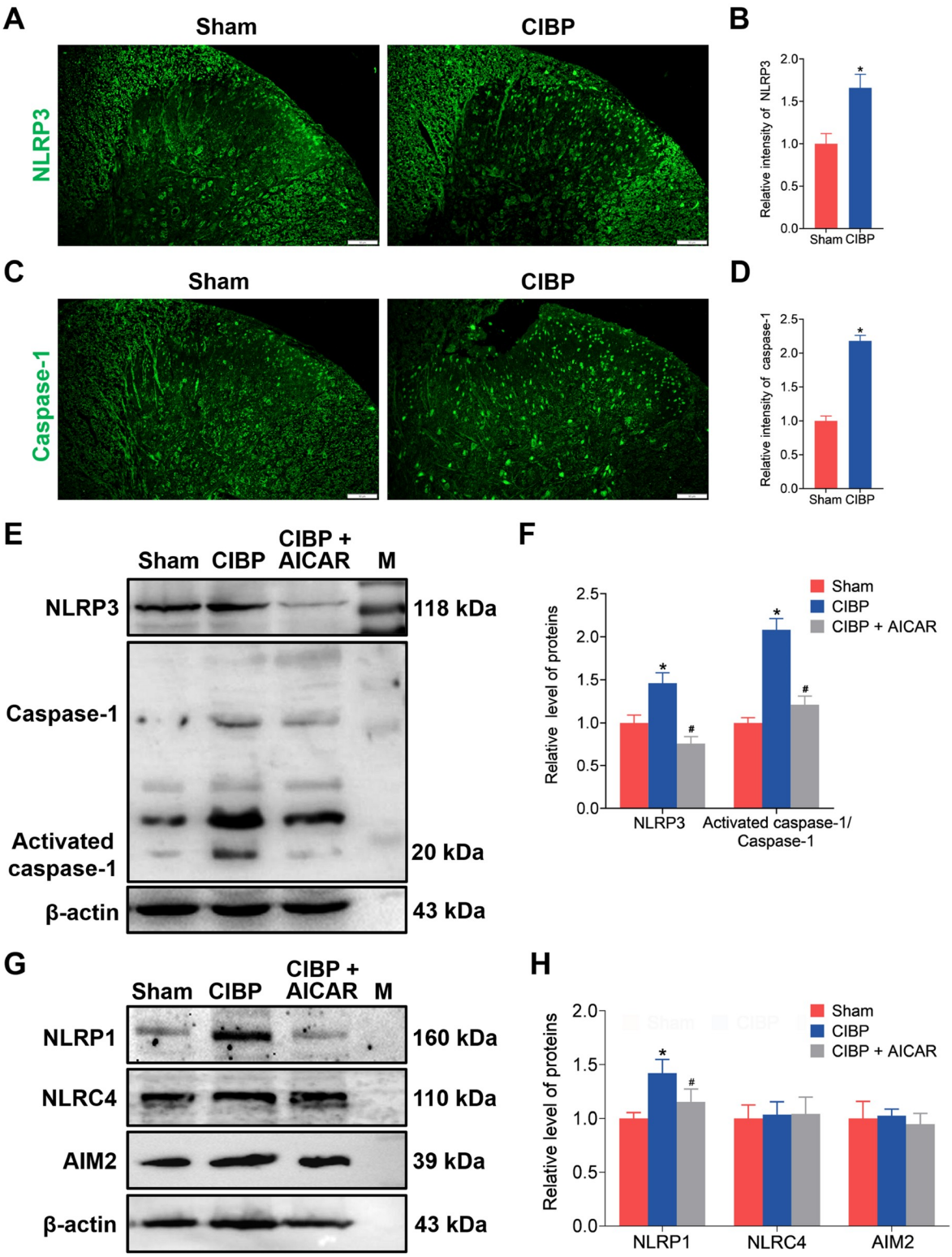

Figure 4. Effect of AICAR treatment on NLRP3, NLRP1, NLRC4, and AIM2 inflammasome components (A,C) Representative immunofluorescence staining images showing the expressions of NLRP3 and caspase-1 in the spinal dorsal horn of sham and CIBP rats. Scale bar: 20 μm. (B,D) Quantitative analysis of fluorescence intensity in (A) and (C). Data are expressed as the mean ± SD ($n = 3$). $^{*}P < 0.05$ vs sham group. (E) Western blot analysis of the levels of NLRP3, caspase-1 and activated caspase-1 in the spinal cord of the sham, CIBP and CIBP + AICAR groups. β-Actin was used as a loading control. (F) Quantification of the relative protein levels in (E). The relative level of activated caspase-1 was normalized to caspase-1. Data are presented as the mean ± SD ($n = 3$). $^{*}P < 0.05$ vs sham group, $^{\#}P < 0.05$ vs CIBP group. (G) Western blot analysis of the levels of NLRP1, NLRC4, and AIM2 in the spinal cord of the sham, CIBP and CIBP + AICAR groups. (H) Quantification of the relative protein levels in (G). Data are presented as the mean ± SD ($n = 3$). $^{*}P < 0.05$ vs sham group, $^{\#}P < 0.05$ vs CIBP group.

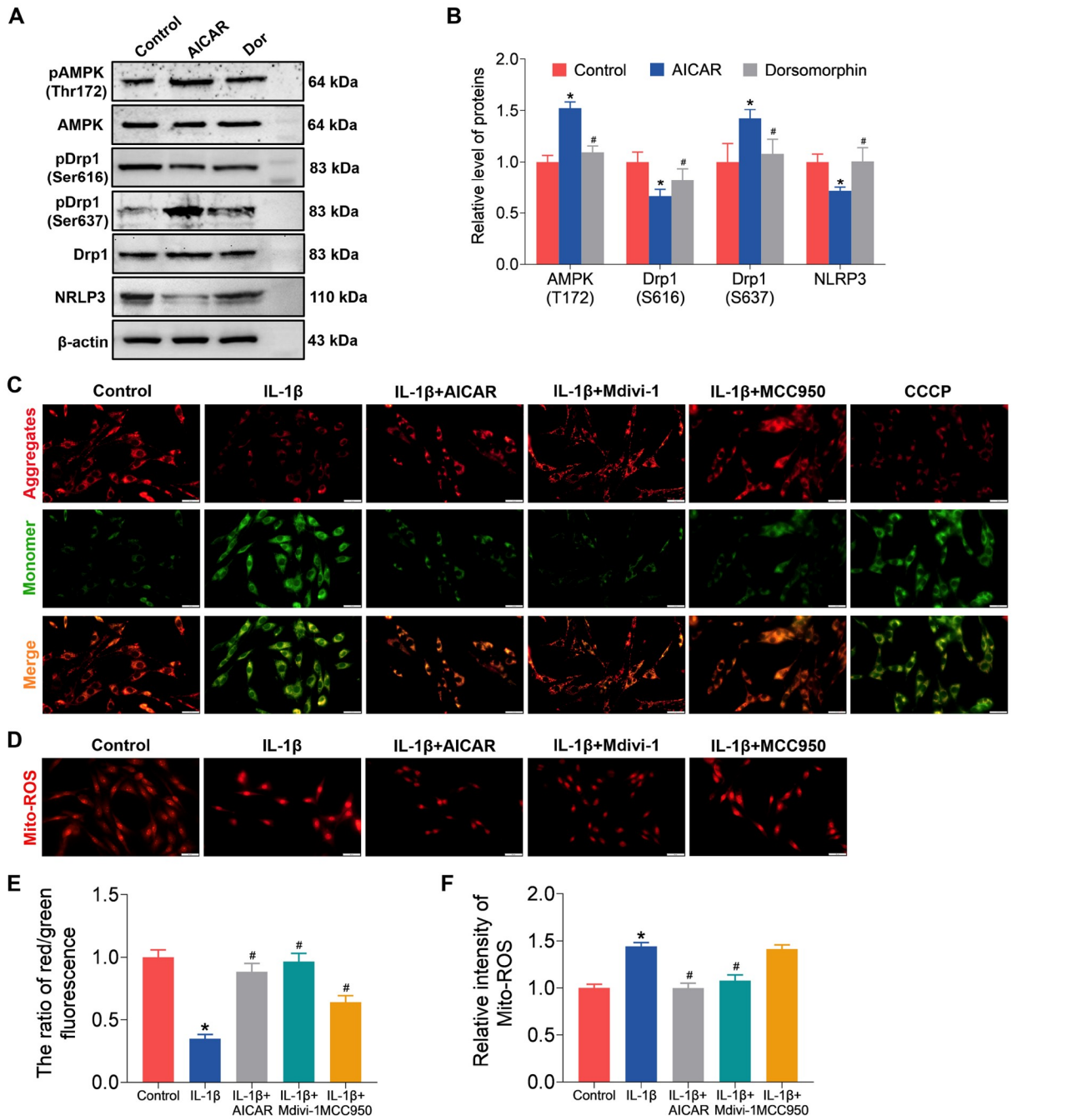

Figure 5. Effect of AICAR and dorsomorphin treatment on mitochondrial membrane potential and mitochondrial ROS in C6 cells (A) Western blot analysis of the levels of phosphorylated AMPK, AMPK, phosphorylated Drp1, Drp1 and NLRP3 in AICAR- or dorsomorphin-treated C6 cells. (B) Quantification of the relative protein levels in (A). The relative level of phosphorylated AMPK was normalized to total AMPK; phosphorylated Drp1 was normalized to total Drp1. Data are presented as the mean ± SD ($n = 3$). $^{*}P < 0.05$ vs Control group, $^{\#}P < 0.05$ vs AICAR group. (C) Representative fluorescence images of JC-1 in the control, IL-1β, IL-1β + AICAR, IL-1β + Mdivi-1, and IL-1β + MCC950 groups. Red fluorescence indicates JC-1 aggregates representing an increase in mitochondrial membrane potential. The green fluorescence indicates the JC-1 monomer, representing a reduction in mitochondrial membrane potential. CCCP was used as a positive control. (D) Representative fluorescence images of Mito-ROS in the control, IL-1β, IL-1β + AICAR, IL-1β + Mdivi-1, and IL-1β + MCC950 groups. (E) Quantitative analysis of the ratio of red/green fluorescent intensity. Data are shown as the mean ± SD ($n = 3$). $^{*}P < 0.05$ vs control group, $^{\#}P < 0.05$ vs IL-1β group. Scale bar: 20 μm. (F) Quantitative analysis of fluorescence intensity in D. Data are shown as the mean ± SD ($n = 3$). $^{*}P < 0.05$ vs control group, $^{\#}P < 0.05$ vs IL-1β. Scale bar: 20 μm.

During pathological pain processing, spinal glial cells are robustly activated and are in a resting state under physiological conditions [21]. These activated glial cells modulate synaptic transmission efficiency and synaptic plasticity by regulating dendritic spine structure. Moreover, glial cells release proinflammatory factors such as TNF-α and IL-1β to strengthen synapse excitation and maintain pain [23]. Activated NLRP3 inflammasomes in microglia and astrocytes promote IL-1β and IL-18 release, which plays a vital

role in pathophysiological pain [24]. Activated NLRP3 recruits apoptosis-associated speck-like protein containing a CARD (ASC) and caspase-1 to form the NLRP3 inflammasome, which mediates caspase-1 activation. Consequently, activated caspase-1 cleaves IL-1β for maturation and cleaves the pore-forming protein gasdermin D (GSDMD) to form membrane pores for cytokine release [25]. In the current research, upregulated mechanical allodynia and spontaneous pain in CIBP rats (Figure 1) were accompanied by the activation of NLRP3 inflammasome-mediated neuroinflammation in the spinal cord (Figure 4). These findings suggested that NLRP3-mediated inflammatory signaling contributed to increased pain sensitivity. A large body of research indicates that NLRP3 is a potential target for the treatment of chronic pain. The activation of the NLRP3 inflammasome is found in nerve injury-induced neuropathic pain, chemotherapy-induced peripheral neuropathy, inflammatory pain, and cancer-related pain, and pharmacological inhibition, and downregulation of the NLRP3 inflammasome-mediated inflammatory response can alleviate pain behaviors [24,26,27]. Accordingly, our observation that AICAR treatment reduced the pain sensitivity of CIBP rats (Figure 1) and inhibited the NLRP3 inflammasome (Figure 4) indicated that AMPK is involved in the activation of NLRP3 inflammatory signal-induced pain in CIBP rats. Therefore, reducing neuroinflammation in the spinal cord could be an effective strategy to relieve pain in CIBP rats.

A series of studies have demonstrated that AMPK is involved in the modulation of chronic pain, such as inflammatory pain, neuropathic pain and osteoarthritis (OA) pain. Activation of the AMPK-mediated signaling pathway in these pain models has inhibitory effects on pain behaviors [17,28,29]. Treatment with the AMPK activator AICAR attenuated CFA-induced inflammatory pain by inhibiting nuclear factor kappa-B (NF-κB) signaling [17]. Another study revealed that in the spinal cord of OA rats, activation of AMPK/peroxisome proliferator-activated receptor γ coactivator 1 α (PGC-1α) contributed to ameliorating mechanical allodynia [28]. Our findings that both phosphorylated AMPK and Drp1 levels were changed in CIBP rats implied the correlative relationship between AMPK and mitochondrial function (Figure 3). AMPK activation plays a critical role in maintaining mitochondrial function and inhibiting the inflammatory response. AMPK activation promotes mitochondrial biogenesis by increasing nuclear respiratory factor 1 activity and PGC-1α expression. Mice expressing a dominant-negative AMPK mutant failed to induce mitochondrial biogenesis [30]. Abnormal regulation of AMPK functions in mitochondrial damage. Pharmacological activation of AMPK by A-769662 or AICAR directly phosphorylates mitochondrial fission factor (MFF) and Drp1 and triggers mitochondrial fission [31]. In AMPKα2-null mice, Drp1 protein levels are increased and trigger mitochondrial fission [30]. Moreover, silencing of *AMPK* reduced Drp1 phosphorylation at Ser637 [32]. Drp1-mediated mitochondrial fission depends on the phosphorylation of Drp1 at different sites, which is regulated by several kinases, such as protein kinase A (PKA), PTEN-induced putative kinase 1 (PINK1), Cyclin-dependent kinase 5 (CDK5) and CDK1/cyclin B [33,34]. Among them, PKA can differentially regulate the phosphorylation of Drp1 at Ser637 and Ser616. Forskolin (a potent adenylate cyclase activator) induces the activation of PKA and stimulates Drp1 phosphorylation at Ser637 and dephosphorylation at Ser616. Overexpression of a PKA inhibitor restores the Drp1 phosphorylation state induced by forskolin [35]. In our research, enhanced phosphorylation of Drp1 at Ser616 and decreased phosphorylation of Drp1 at Ser637 were observed in CIBP rats, while this imbalance was restored by AICAR treatment (Figure 3F,G), which indicated that AMPK activation could influence Drp1 activity. This effect is probably not direct because of the interactions between AMPK and PKA, as proven by AICAR-treated cells showing increased PKA activity [36]. Therefore, AMPK activation improved the dysregulation of Drp1 in CIBP rats, which could probably be mediated by the interaction of AMPK and PKA.

AMPK serves as a mitochondrial guardian by influencing mitochondrial ATP production and ROS generation. AMPK activation increases uncoupling protein 2 (UCP2) expression and suppresses protein kinase C to reduce the level of mitochondria-generated ROS [37]. In the current study, deficient mitochondrial structure and abnormal phosphorylated Drp1 in the spinal cord of CIBP rats indicated that mitochondrial dysfunction is involved in the pathological characteristics of CIBP (Figure 3). A similar phenomenon was also found in other pathological models. Enhanced PGC-1α-mediated mitochondrial biogenesis in the spinal cord had an analgesic effect on paclitaxel-induced neuropathic pain rats [38]. In addition to mitochondrial biogenesis, an imbalance in mitochondrial fission and fusion was induced by treatment with the chemotherapy drug vincristine. The mitochondrial-targeted antioxidant mitoquinone alleviated chemotherapy pain by improving mitochondrial dysfunction [39]. As highly dynamic organelles, mitochondria undergo fusion and fission. The dynamic balance between fission and fusion maintains the distribution, morphology, and number of mitochondria and plays a vital role in mitochondrial function. Disruption of the mitochondrial fission-fusion balance leads to the accumulation of either fragmented or hyperfused mitochondria, causing mitochondrial dysfunction. Drp1 is known as the central mediator of mitochondrial fission and is recruited to punctate spots on the mitochondrial surface to promote fission [18]. In the present study, we found that Drp1 was overexpressed and activated in the spinal cord of CIBP rats (Figure 3B,F), which suggested that cancer bone metastasis induced spinal mitochondrial fission-mediated dysfunction. Mitochondrial damage and ROS production are the main mediators of NLRP3 inflammasome activation [40]. Mitochondrial dysfunction contributes to the production of ROS, which further promotes the activation of the NLRP3 inflammasome and leads to neuroinflammation [41]. Drp1 not only mediates ROS generation in the normal state but also leads to additional ROS production by inducing excess mitochondrial fission. Excess ROS production contributes to mitochondrial damage and is consequently implicated in the pathogenesis of neurological diseases [42]. Taken together, the observation of mitochondrial damage-associated neuroinflammation mainly occurs because of the disruption of mitochondrial redox imbalance induced by Drp1-mediated mitochondrial fragmentation.

In conclusion, the activation of AMPK by AICAR reduces Drp1-mediated mitochondrial fission and dysfunction and inhibits NLRP3 inflammasome-mediated neuroinflammation, which consequently attenuates cancer-induced bone pain (Figure 6).

Funding

This work was supported by the grants from the National Natural Science Foundation of China (Nos. 81971066, 81901149, and 32100823), the Research Project of Hubei Provincial Department of Education (No. Q20212804), and the Hubei University of Science

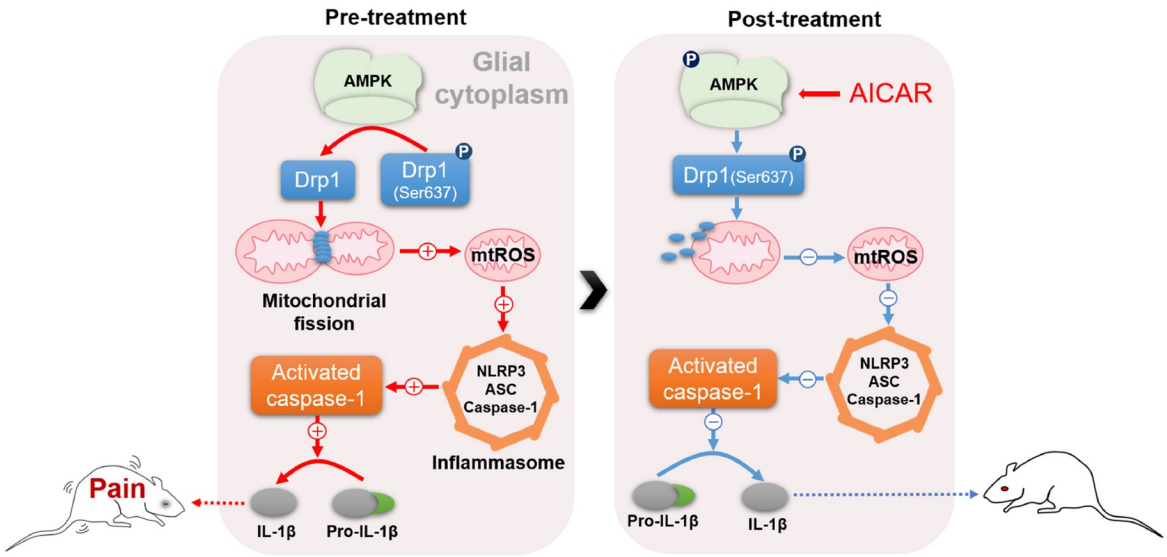

Figure 6. Schematic representation of the potential mechanisms by which AICAR treatment reduces spinal inflammation and alleviates cancer-induced bone pain Activation of AMPK by AICAR inhibits mitochondrial fission and NLRP3 inflammasome activity and consequently reduces IL-1β expression in the spinal cord of CIBP rats. The decreased expression of proinflammatory cytokine is relevant to the downregulated pain sensitivity in CIBP rats. Accordingly, AICAR treatment has an analgesia effect on CIBP rats.

and Technology Program (Nos. 2020TD02, BK202116, and 2020XZ40).

Conflict of Interest

The authors declare that they have no conflict of interest.

References

1. Sung H, Ferlay J, Siegel RL, Laversanne M, Soerjomataram I, Jemal A, Bray F. Global cancer statistics 2020: GLOBOCAN estimates of incidence and mortality worldwide for 36 cancers in 185 countries. *CA Cancer J Clin* 2021, 71: 209–249
2. Xia C, Dong X, Li H, Cao M, Sun D, He S, Yang F, *et al.* Cancer statistics in China and United States, 2022: profiles, trends, and determinants. *Chin Med J* 2022, 135: 584–590
3. Ellingson HM, Vanderah TW. Potential therapeutic treatments of cancer-induced bone pain. *Curr Opin Supportive Palliative Care* 2020, 14: 107–111
4. Zheng XQ, Wu Y, Huang J, Wu AM. Neurophysiological mechanisms of cancer-induced bone pain. *J Adv Res* 2021, 35: 117–127
5. Onishi M, Yamano K, Sato M, Matsuda N, Okamoto K. Molecular mechanisms and physiological functions of mitophagy. *EMBO J* 2021, 40: e104705
6. Ji RR, Xu ZZ, Gao YJ. Emerging targets in neuroinflammation-driven chronic pain. *Nat Rev Drug Discov* 2014, 13: 533–548
7. Teixeira-Santos L, Albino-Teixeira A, Pinho D. Neuroinflammation, oxidative stress and their interplay in neuropathic pain: focus on specialized pro-resolving mediators and NADPH oxidase inhibitors as potential therapeutic strategies. *Pharmacol Res* 2020, 162: 105280
8. Hess A, Axmann R, Rech J, Finzel S, Heindl C, Kreitz S, Sergeeva M, *et al.* Blockade of TNF-α rapidly inhibits pain responses in the central nervous system. *Proc Natl Acad Sci USA* 2011, 108: 3731–3736
9. Shi Y, Gelman BB, Lisinicchia JG, Tang SJ. Chronic-pain-associated astrocytic reaction in the spinal cord dorsal horn of human immunodeficiency virus-infected patients. *J Neurosci* 2012, 32: 10833–10840
10. Xie M, Cheng M, Wang B, Jiao M, Yu L, Zhu H. 2-Bromopalmitate attenuates inflammatory pain by maintaining mitochondrial fission/fusion balance and function. *Acta Biochim Biophys Sin* 2021, 53: 72–84
11. Li MY, Ding JQ, Tang Q, Hao MM, Wang BH, Wu J, Yu LZ, *et al.* SIRT1 activation by SRT1720 attenuates bone cancer pain via preventing Drp1-mediated mitochondrial fission. *Biochim Biophys Acta Mol Basis Dis* 2019, 1865: 587–598
12. van der Vlist M, Raoof R, Willemen HLDM, Prado J, Versteeg S, Martin Gil C, Vos M, *et al.* Macrophages transfer mitochondria to sensory neurons to resolve inflammatory pain. *Neuron* 2022, 110: 613–626.e9
13. Doyle TM, Salvemini D. Mini-Review: mitochondrial dysfunction and chemotherapy-induced neuropathic pain. *Neurosci Lett* 2021, 760: 136087
14. Shi Y, Yuan S, Tang SJ. Reactive oxygen species (ROS) are critical for morphine exacerbation of HIV-1 gp120-induced pain. *J Neuroimmune Pharmacol* 2021, 16: 581–591
15. Song H, Han Y, Pan C, Deng X, Dai W, Hu L, Jiang C, *et al.* Activation of adenosine monophosphate-activated protein kinase suppresses neuroinflammation and ameliorates bone cancer pain. *Anesthesiology* 2015, 123: 1170–1185
16. Hao M, Tang Q, Wang B, Li Y, Ding J, Li M, Xie M, *et al.* Resveratrol suppresses bone cancer pain in rats by attenuating inflammatory responses through the AMPK/Drp1 signaling. *Acta Biochim Biophys Sin* 2020, 52: 231–240
17. Xiang HC, Lin LX, Hu XF, Zhu H, Li HP, Zhang RY, Hu L, *et al.* AMPK activation attenuates inflammatory pain through inhibiting NF-κB activation and IL-1β expression. *J Neuroinflammation* 2019, 16: 34
18. Matsuda M, Huh Y, Ji RR. Roles of inflammation, neurogenic inflammation, and neuroinflammation in pain. *J Anesth* 2019, 33: 131–139
19. O'Brien WT, Pham L, Symons GF, Monif M, Shultz SR, McDonald SJ. The NLRP3 inflammasome in traumatic brain injury: potential as a biomarker and therapeutic target. *J Neuroinflammation* 2020, 17: 104
20. Seager R, Lee L, Henley JM, Wilkinson KA. Mechanisms and roles of mitochondrial localisation and dynamics in neuronal function. *Neuronal Signal* 2020, 4: NS20200008
21. Oostinga D, Steverink JG, van Wijck AJM, Verlaan JJ. An understanding of bone pain: a narrative review. *Bone* 2020, 134: 115272
22. Feller L, Khammissa RAG, Bouckaert M, Ballyram R, Jadwat Y, Lemmer J.

Pain: Persistent postsurgery and bone cancer-related pain. *J Int Med Res* 2019, 47: 528–543
23. Wright-Jin EC, Gutmann DH. Microglia as dynamic cellular mediators of brain function. *Trends Mol Med* 2019, 25: 967–979
24. Chen R, Yin C, Fang J, Liu B. The NLRP3 inflammasome: an emerging therapeutic target for chronic pain. *J Neuroinflammation* 2021, 18: 84
25. Wang Z, Zhang S, Xiao Y, Zhang W, Wu S, Qin T, Yue Y, *et al.* NLRP3 inflammasome and inflammatory diseases. *Oxid Med Cell Longev* 2020, 2020: 1–11
26. Chen SP, Zhou YQ, Wang XM, Sun J, Cao F, HaiSam S, Ye DW, *et al.* Pharmacological inhibition of the NLRP3 inflammasome as a potential target for cancer-induced bone pain. *Pharmacol Res* 2019, 147: 104339
27. Li Z, Zhu J, Wang Y. ADAR3 alleviated inflammation and pyroptosis of neuropathic pain by targeting NLRP3 in chronic constriction injury mice. *Gene* 2021, 805: 145909
28. Sun J, Song FH, Wu JY, Zhang LQ, Li DY, Gao SJ, Liu DQ, *et al.* Sestrin2 overexpression attenuates osteoarthritis pain via induction of AMPK/PGC-1α-mediated mitochondrial biogenesis and suppression of neuroinflammation. *Brain Behav Immun* 2022, 102: 53–70
29. Baeza-Flores GDC, Guzmán-Priego CG, Parra-Flores LI, Murbartián J, Torres-López JE, Granados-Soto V. Metformin: a prospective alternative for the treatment of chronic pain. *Front Pharmacol* 2020, 11: 558474
30. Wu S, Zou MH. AMPK, mitochondrial function, and cardiovascular disease. *Int J Mol Sci* 2020, 21: 4987
31. Garcia D, Shaw RJ. AMPK: mechanisms of cellular energy sensing and restoration of metabolic balance. *Mol Cell* 2017, 66: 789–800
32. Li Y, Zhou ZH, Chen MH, Yang J, Leng J, Cao GS, Xin GZ, *et al.* Inhibition of Mitochondrial Fission and NOX2 Expression Prevent NLRP3 inflammasome activation in the endothelium: the role of corosolic acid action in the amelioration of endothelial dysfunction. *Antioxid Redox Signal* 2016, 24: 893–908
33. Chang CR, Blackstone C. Cyclic AMP-dependent protein kinase phosphorylation of Drp1 regulates its GTPase activity and mitochondrial morphology. *J Biol Chem* 2007, 282: 21583–21587
34. Knott AB, Perkins G, Schwarzenbacher R, Bossy-Wetzel E. Mitochondrial fragmentation in neurodegeneration. *Nat Rev Neurosci* 2008, 9: 505–518
35. Plewes MR, Hou X, Talbott HA, Zhang P, Wood JR, Cupp AS, Davis JS. Luteinizing hormone regulates the phosphorylation and localization of the mitochondrial effector dynamin-related protein-1 (DRP1) and steroidogenesis in the bovine corpus luteum. *FASEB J* 2020, 34: 5299–5316
36. Stone JD, Narine A, Tulis DA. Inhibition of vascular smooth muscle growth via signaling crosstalk between AMP-activated protein kinase and cAMP-dependent protein kinase. *Front Physio* 2012, 3: 409
37. Jadiya P, Garbincius JF, Elrod JW. Reappraisal of metabolic dysfunction in neurodegeneration: focus on mitochondrial function and calcium signaling. *Acta Neuropathol Commun* 2021, 9: 124
38. Chen N, Ge MM, Li DY, Wang XM, Liu DQ, Ye DW, Tian YK, *et al.* β2-adrenoreceptor agonist ameliorates mechanical allodynia in paclitaxel-induced neuropathic pain via induction of mitochondrial biogenesis. *Biomed Pharmacother* 2021, 144: 112331
39. Chen XJ, Wang L, Song XY. Mitoquinone alleviates vincristine-induced neuropathic pain through inhibiting oxidative stress and apoptosis via the improvement of mitochondrial dysfunction. *Biomed Pharmacother* 2020, 125: 110003
40. Wei S, Ma W, Li X, Jiang C, Sun T, Li Y, Zhang B, *et al.* Involvement of ROS/NLRP3 inflammasome signaling pathway in doxorubicin-induced cardiotoxicity. *Cardiovasc Toxicol* 2020, 20: 507–519
41. Yao X, Carlson D, Sun Y, Ma L, Wolf SE, Minei JP, Zang QS. Mitochondrial ROS induces cardiac inflammation via a pathway through mtDNA damage in a pneumonia-related sepsis model. *PLoS ONE* 2015, 10: e0139416
42. Dai CQ, Guo Y, Chu XY. Neuropathic pain: the dysfunction of drp1, mitochondria, and ROS homeostasis. *Neurotox Res* 2020, 38: 553–563